

## Tunable Surface Phases in Alcohol-Diol Melts

O. Gang,<sup>1</sup> B. M. Ocko,<sup>2</sup> X. Z. Wu,<sup>3</sup> E. B. Sirota,<sup>4</sup> and M. Deutsch<sup>1,\*</sup>

<sup>1</sup>Physics Department, Bar Ilan University, Ramat Gan 52900, Israel

<sup>2</sup>Physics Department, Brookhaven National Laboratory, Upton, New York 11973

<sup>3</sup>IBM Almaden Research Center, San Jose, California 95120

<sup>4</sup>Exxon Research and Engineering Company, Route 22E, Annandale, New Jersey 08801

(Received 11 September 1998)

Surface crystallization is studied in mixed alcohol-diol melts by x-ray diffraction and surface tensiometry. A reversible transition, having no bulk counterpart, from a bilayer to a monolayer surface phase, tunable by either diol concentration  $\phi$  or temperature  $T$ , is observed. The molecular tilt is found to vary with  $\phi$  in the bilayer phase. The structure of both surface phases is determined in detail. A simple theory, assuming a linearized  $\phi$  dependence of the free energies of the various interfaces in each phase, accounts well for the observed  $(\phi, T)$  phase diagram. [S0031-9007(98)08262-3]

PACS numbers: 68.10.-m, 61.25.Em, 64.70.Dv

Chain molecule (normal-alkanes, alkenes, alcohols, etc.) melts were recently shown [1–4] to exhibit surface freezing, i.e., the coexistence of a crystalline surface layer with a liquid bulk, up to a few degrees above the freezing point  $T_f$ . In contrast with traditional quasi-2D systems like Langmuir films on water, the surface-frozen layer consists of the same molecules as the subphase and can, therefore, exchange molecules with it. It is not constrained externally to be quasi-2D, but does so *spontaneously* under the balance of the intermolecular interactions, thermal motion, and surface field. It is, therefore, intermediate between two and three dimensions. Phase transitions in such layers are of great interest by their own right, and also because they provide insight into the dimensional dependence of phase transitions in general. Nevertheless, only two structural transitions, both rotator-to-crystal, were reported to date in these layers: a chain-length ( $n$ ) driven one at  $n \approx 44$  [3] in pure alkanes, and a concentration driven one (over a very limited range) in a  $C_{36}H_{74}:C_{26}H_{54}$  alkane mixture [5].

Alcohols,  $CH_3(CH_2)_{n-1}OH$  (denoted  $C_nOH$ ), whose surface-frozen layers exhibit a more complex structure than alkanes, are particularly useful for studying structural transitions [4,6]. Their surface layer is a hexagonally packed bilayer, with the hydroxyl groups of both upper and lower layers pointing to the center. A previous study of hydrated alcohols [6,7] demonstrated the importance of hydrogen bonding (HB) between the hydroxyl groups in stabilizing the surface-frozen bilayer's structure. In the present study the HB was tuned by mixing a short diol molecule, 1,3-propanediol:  $OH-(CH_2)_3-OH$  (denoted PD), in the alcohol. We show that a reversible transition from a bilayer to a monolayer is induced in the surface layer by varying either the diol mass concentration  $\phi$  or temperature  $T$ , for a range of  $T$  and  $\phi$ . More subtle effects, like a continuous change in the molecular tilt with  $\phi$  in the bilayer phase, are also observed, showing that the interlayer interactions influence the intralayer structure

significantly. Finally, the observed  $(\phi, T)$  surface phase diagram is accounted for quantitatively within a simple theory, based on the surface free energy balance in each phase.

Alcohol/PD mixtures, made of  $>99\%$  pure commercial material, were studied for  $18 \leq n \leq 28$  and  $\phi \leq 0.23$ . An  $\sim 0.5$  g sample was spread on a copper wafer inside a sealable, temperature controlled ( $\leq 0.005^\circ C$ ) cell, mounted on the liquid surface diffractometer at beam line X22B, NSLS, Brookhaven National Laboratory. X-ray reflectivity (XR), grazing incidence diffraction (GID), and Bragg rods (BR) measurements were employed to study, respectively, the surface-normal density profile (XR), the surface-parallel crystalline packing (GID), and molecular tilt (BR) vs  $T$ . Surface thermodynamics were probed by surface tension (ST),  $\gamma(T)$ , measurements, using the Wilhelmy plate method [2]. For further details see [3].

A 90%  $C_{22}OH:10\%$  PD ST curve is shown in Fig. 1. The slope  $d\gamma(T)/dT = \Delta S = -(S_{\text{surf}} - S_{\text{bulk}})$ , where  $\Delta S$  is the surface-bulk entropy difference [2]. For a liquid surface  $S_{\text{surf}} > S_{\text{bulk}}$  and  $d\gamma(T)/dT < 0$ . Upon cooling the surface freezes at  $T_{s1} = 69.7^\circ C$ , making  $S_{\text{surf}} < S_{\text{bulk}}$  and  $d\gamma(T)/dT > 0$ . The observed change,  $\Delta[d\gamma(T)/dT] \approx 1$  mN/(m $^\circ C$ ), is close to that of an alkane of equal length, and thus indicates that a crystalline surface *monolayer* [3] is likely formed. Cooling further, an abrupt slope doubling, to  $d\gamma(T)/dT \approx 2$  mN/(m $^\circ C$ ), is observed at  $T_{s2} = 66.7^\circ C$ . This suggests a transition to a crystalline surface *bilayer*, with a slope identical with that of a pure alcohol of equal length [6]. The measured XR vs  $T$  at a fixed wave vector,  $q_z = 0.25 \text{ \AA}^{-1}$  (solid line in Fig. 1), shows two abrupt jumps, coinciding with the slope changes of the ST scan. They demonstrate dramatically the existence and first-order nature of the two surface phase transitions. Moreover, the constant XR between the jumps shows that no other changes occur in the surface layer's structure. At  $T_f$  (bulk freezing) the surface roughens macroscopically [1] and the XR drops abruptly to near zero.

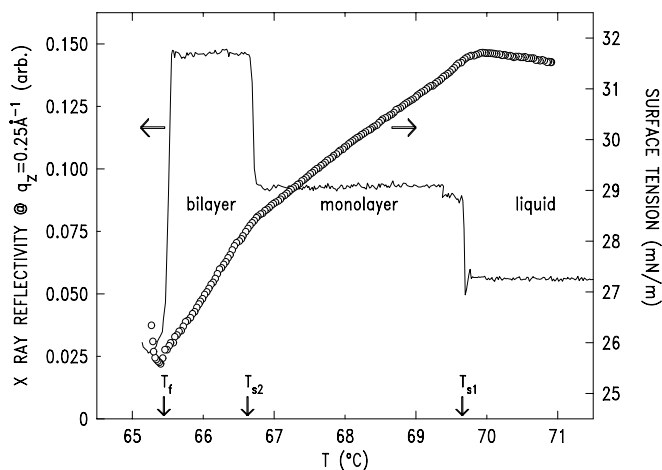


FIG. 1. Surface tension (ST) (points), and x-ray reflectivity (XR) at a fixed wave vector  $q_z = 0.25 \text{ \AA}^{-1}$  (line) scans for a 90%  $\text{C}_{24}\text{OH}$ :10% PD. The slope changes (ST) and intensity jumps (XR) denote the liquid/monolayer ( $T_{s1} = 69.7 \text{ }^\circ\text{C}$ ) and monolayer/bilayer ( $T_{s2} = 66.7 \text{ }^\circ\text{C}$ ) surface phase transitions.  $T_f = 65.4 \text{ }^\circ\text{C}$  is the bulk freezing temperature.

Figure 2 shows measured reflectivity curves for pure  $\text{C}_{24}\text{OH}$  (a) and 90%  $\text{C}_{24}\text{OH}$ :10% PD for different surface phases (b)–(d). The Kiessig fringes in curves (a)–(c) indicate a thin surface layer of electron density different from the bulk. For (c) the longer modulation period,  $\Delta q_z$ , indicates a thinner layer. A careful comparison reveals also a slightly smaller  $\Delta q_z$  for (b) than for (a), indicating a thicker layer. The monotonically decreasing

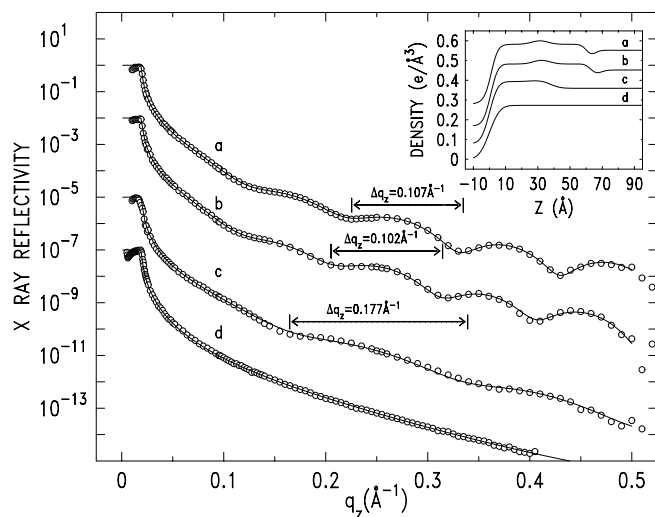


FIG. 2. X-ray reflectivity for the bilayer phases of pure  $\text{C}_{24}\text{OH}$  (a) and a 90%  $\text{C}_{24}\text{OH}$ :10% PD mixture (b), the monolayer phase of the mixture (c), and the liquid surface phase of the mixture (d). The lines are fits to the models discussed in the text, and the inset shows the corresponding surface-normal electron density profiles. The reflectivity curves are shifted vertically for clarity by 2 (b), 5 (c), and 7 (d) decades and the density curves in the inset by 0.28 (a), 0.18 (b), and 0.08 (c)  $e/\text{\AA}^3$ .

curve (d), measured at  $T \gg T_{s1} = 69.7 \text{ }^\circ\text{C}$ , is typical for an unstructured liquid surface.

To derive detailed surface-normal density profiles  $\rho(z)$ , a 5-slab model [3,6] was fitted to curves (a) and (b) by the widely used matrix method [8,9]. The model comprises the top monolayer's (1)  $\text{CH}_3$  end group layer and (2)  $(\text{CH}_2)_{n-1}$  alkyl chain layer, (3) the top and bottom monolayers' OH groups, and the bottom monolayer's (4)  $(\text{CH}_2)_{n-1}$  alkyl chain layer and (5)  $\text{CH}_3$  end group layer. To minimize the number of fit parameters, slabs (1) and (5) were constrained to be identical, and so were (2) and (4). No other constraints were employed. As each slab has a density and a thickness, six parameters plus a single Gaussian roughness parameter common to all slabs were refined in the fit. For further information see Refs. [4,6,7]. The fit to (a) (line), and the corresponding  $\rho(z)$  in the inset, are typical of a surface-frozen alcohol bilayer [6], with a high-density OH layer at the center, and a thickness  $d = 62.6 \text{ \AA}$ . As shown earlier [4,6], the  $\text{C}_{24}\text{OH}$  molecules in the bilayer are tilted from the surface normal towards their next-nearest neighbors (NNN) by  $16^\circ$ . This, along with the  $\sim 32 \text{ \AA}$  length calculated for the extended molecule yields a calculated layer thickness of  $61.5 \text{ \AA}$ , in good agreement with the XR-fitted value. A fit of the same model to the mixture (b) yields, again, a bilayer. It is, however,  $\sim 2.2 \text{ \AA}$  thicker than for pure  $\text{C}_{24}\text{OH}$ , due to a molecular tilt decrease, as shown below.

For curve (c) of Fig. 2 a 2-slab model is employed, representing the  $\text{CH}_3(\text{CH}_2)_{n-1}$  and OH layers, respectively. Thus, four parameters plus a common roughness parameter were employed in the fit. The resultant density profile, (c), indeed confirms the surface layer to be a monolayer with  $d \approx 32 \text{ \AA}$ . Its vapor side is identical with that of the bilayer (b). Its liquid side, however, is markedly different. The OH slab obtained here, as for all other chain lengths [6], is thicker by  $\sim 5 \text{ \AA}$  than a single OH slab in the bilayer model. When smeared with the interface's Gaussian roughness it yields a tail, decreasing gradually from the high density of the OH slab to that of the bulk liquid, as is seen clearly at  $32 \leq z \leq 42 \text{ \AA}$  in (c). A possible mechanism for the formation of this tail is PD adsorption on the ordered OH bottom surface of the monolayer, which is a weakly attractive substrate [10] for OH groups. As PD has 16-fold more OH groups *per carbon* than  $\text{C}_{24}\text{OH}$ , PD will adsorb preferentially onto the monolayer's lower surface. Assuming an equal adsorption probability for each bulk OH group, regardless of the molecule it is attached to, a  $\phi \approx 8\%$  of PD suffices to cover 2/3 of the monolayer's bottom by PD molecules. The higher electron density of the PD molecules, as compared to alcohols, results in the higher-density tail extending below the monolayer.

GID [Figs. 3(a)–3(c)] yields a single peak at  $q_{\parallel} \approx 1.49 \text{ \AA}^{-1}$  for the pure material (a) and both phases of the mixture (b),(c). Isolating the diffraction from a single surface crystallite by a careful alignment of a high-resolution collimator consisting of two

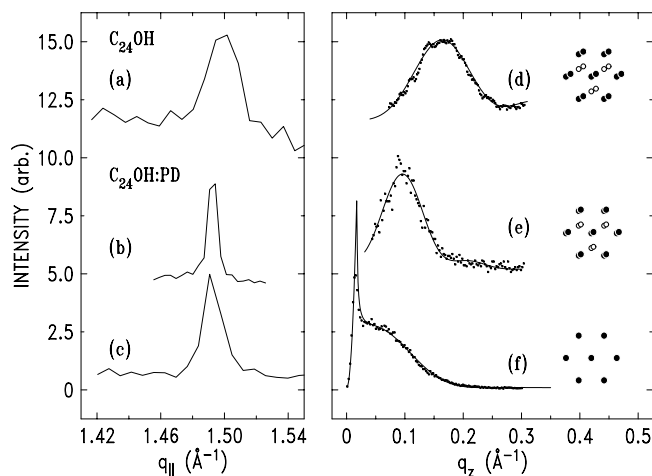


FIG. 3. Grazing incidence diffraction (a)–(c) and Bragg rods (d)–(f) measured for the bilayer phase in pure  $C_{24}OH$  (a),(d), in a 90%  $C_{24}OH$ :10% PD mixture (b),(e), and in the monolayer phase of the mixture (c),(f). The lines in (d)–(f) are fits to the measured data (points). The insets show the in-plane packing and molecular tilts, with closed points representing molecules in the upper layer and open ones—in the lower layer.

well-separated sets of slits on the detector arm of the diffractometer reveals that this peak repeats upon a  $60^\circ$  sample rotation. This and the fact that only a single GID peak is found indicate a hexagonal crystalline order within the layer, with a molecular area  $A = 20.3 \text{ \AA}^2$ . The peaks of the mixture (b),(c) are narrower than those of the pure  $C_{24}OH$  (a), indicating a larger crystalline coherence length, of order  $1000 \text{ \AA}$ , as compared to the few hundred  $\text{Å}$  of pure  $C_{24}OH$ . Alternatively, the pure  $C_{24}OH$  peak may be a composite of two unresolved peaks. The corresponding Bragg rods, and their fits [3,6], are shown in Figs. 3(d)–3(f). Those of the bilayer (d),(e) are typical of NNN-tilted molecules [4,6], as shown in the inset. The different peak positions,  $q_z = 0.16 \text{ \AA}^{-1}$  (d) and  $q_z = 0.1 \text{ \AA}^{-1}$  (e), indicate, however, considerably different tilt angles. A full-curve fit (lines) yields  $\sim 16^\circ$  for the pure sample and  $9^\circ$  for the mixture, which results in an  $\sim 1.7 \text{ \AA}$  increase in the bilayer thickness. This is equal (within fit errors) to the  $\sim 2.2 \text{ \AA}$  thickness increase observed by XR, indicating that hardly any true swelling, i.e., dilation due to PD intercalation into the bilayer, occurs here. This conclusion is further supported by the XR fits, which yield equal densities and thicknesses for the OH slab at the center of the bilayer for both pure and mixed samples. Moreover, a study of the crystalline bulk's structure just below  $T_f$  [11] also indicates no intercalation of PD molecules into the bilayer's center. This behavior is in contrast with hydrated alcohols, where an intercalation of water molecules into the bilayer was observed for both the surface-frozen bilayer [6], and the bulk [12]. The repulsion between the bilayer's hydrophilic OH groups and the PD's lipophilic hydrocarbon chain probably inhibits the PD intercalation.

Tilt transitions are generally considered to be dominated by in-layer interactions, and strongly depend on chain length [13]. The last is clearly incorrect here, since the pure and mixed samples, having different tilts, consist of the same alcohol molecule. Also, no other structural changes which could induce the tilt variation, like PD intercalation, lattice spacing variations, etc., are observed. Thus, the tilt variation here seems to be driven completely by the bilayer-subphase interaction. The increase in the OH concentration with that of PD renders the subphase more hydrophilic, increasing the repulsion between the subphase and the tilted lipophilic chains in the surface bilayer. The only way for the bilayer to reduce this repulsion short of the total disruption of the surface layer is to decrease the tilt, which increases the distance between the subphase and each  $CH_2$  group of the layer's chain. The reverse effect, an *attraction* induced tilt change, was found for molecules adsorbed onto a solid substrate [14]. Here, however, the tilt angle can be changed continuously, by varying  $\phi$  and the diol's chain length, as we show elsewhere [11].

For  $T_{s2} < T < T_{s1}$  the BR, Fig. 3(f), differs markedly from those of the bilayers (d),(e). The fit (line) yields a thickness of  $34 \pm 1 \text{ \AA}$ , in reasonable agreement with the  $\sim 32 \text{ \AA}$  of XR and the calculated length. The peaking of the BR at  $q_z < 0.04 \text{ \AA}^{-1}$  indicates a molecular tilt  $< 4^\circ$ . Considering the enhanced OH concentration at the subphase/monolayer interface, and the consequent increase in the repulsion between the two, this near-zero tilt supports our conclusion above that the tilt variation originates in the repulsion between the subphase and surface-layer chains.

The measured  $(\phi, \Delta T)$  surface phase diagram (circles) is shown in Fig. 4, where  $\Delta T = T - T_f$ . For  $\phi \leq 0.06$  only the bilayer phase occurs below the liquid phase. For  $0.06 \leq \phi \leq 0.23$  the monolayer phase appears, interposed between the bilayer and liquid surface phases. Its temperature existence range almost doubles with  $\phi$  from  $\Delta T(\phi \approx 0.1) = 2^\circ\text{C}$  to  $\Delta T(\phi \approx 0.2) = 3.6^\circ\text{C}$ . The bilayer's  $\Delta T$  decreases slightly over the same  $\phi$  range. Around  $\phi \approx 0.23$  macroscopic phase separation occurs, preventing meaningful measurements at higher  $\phi$ . We now show that this diagram can be accounted for quantitatively assuming a linear  $\phi$  dependence for the surface energies associated with the various interfaces in the system, marked on the cartoons in the figure. The total free energy  $F$  is first calculated for each phase using these surface energies. Then, equating pairs of free energies yields the transition temperatures vs composition, i.e., the phase boundaries.

For the liquid surface:  $F_{liq} = \gamma_{vl}$ . Upon mixing with the higher-ST diol,  $\gamma_{vl}$  is assumed to increase linearly from the pure sample's value,  $\gamma_{vl}^p$ , as  $\gamma_{vl}(\phi) = \gamma_{vl}^p + D\phi$ , where  $D$  is a constant. For  $T < T_{s1}$  a monolayer exists at the surface, with OH headgroups pointing into the liquid and hydrocarbon tails pointing into the vapor

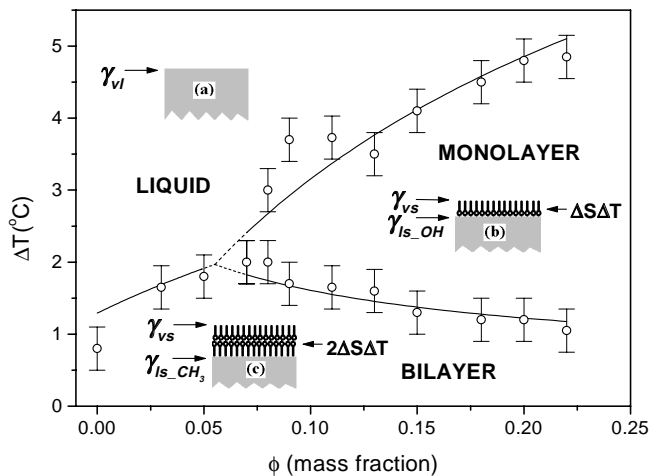


FIG. 4. The surface phase diagram of the  $C_{24}OH:PD$  mixture melt. Open circles denote measured values. The lines are fits to the theory discussed in the text. The cartoons (a)–(c) schematize the molecular packing of the surface layers and show the various surface energies.

[see cartoon in Fig. 4(b)]. The corresponding two interfaces,  $CH_3/vapor$  and  $OH/liquid$ , have surface energies  $\gamma_{vs}$  and  $\gamma_{ls-OH}$ , respectively.  $\gamma_{vs}$  is assumed to be  $\phi$  independent.  $\gamma_{ls-OH}$ , however, is large for small  $\phi$ , due to the strong repulsion between the OH head-group and the predominantly hydrocarbonic liquid, but *decreases* rapidly with increasing  $\phi$ , due to the OH concentration increase in the bulk. Thus,  $\gamma_{ls-OH}(\phi) = \gamma_{vs} + A/(B + \phi)$ . At any  $T \equiv T_f + \Delta T$  the total surface free energy, including the entropy gain  $\Delta S$  upon surface crystallization, is  $F_{mono} = \gamma_{vs} + \gamma_{ls-OH}(\phi) + \Delta S\Delta T$ . For  $T < T_{s2}$ , a bilayer exists at the surface and now a  $CH_3$  group faces the liquid [cartoon in Fig. 4(c)]. The corresponding surface free energy, denoted  $\gamma_{ls-CH_3}$ , is small ( $\sim$ few mN/m) [15] and weakly increasing with  $\phi$ :  $\gamma_{ls-CH_3}(\phi) = \gamma_{ls-CH_3}^p + C\phi$ . The entropy gain upon surface freezing is double that of the monolayer. Thus,  $F_{bi} = \gamma_{vs} + \gamma_{ls-CH_3}(\phi) + 2\Delta S\Delta T$ .

Equating now the free energies of two phases yields expressions for the transition temperatures between them vs  $\phi$ , in terms of the constants above. A fit of the expressions obtained to the measured transition temperatures and average entropy [ $\Delta S = 1.25$  mJ/(m<sup>2</sup> °C)] yields the phase boundaries (lines) in Fig. 4 and the fit parameter values:  $R(\equiv \gamma_{vl}^p - \gamma_{vs} - \gamma_{ls-CH_3}^p) = 3.23$  mN/m,  $A = 1.52$  mN/m,  $B = 0.407$ ,  $C = 0.224$  mN/m, and  $D = 8.66$  mN/m. This  $R$  is in good agreement with the  $\sim 3.5$  mN/m calculated from the measured  $\gamma_{vl}^p = 30.5$  mN/m [6] and  $\gamma_{vs-CH_3} \approx 23$  mN/m and  $\gamma_{ls}^p \approx 4$  mN/m. The last two values, which are not measurable directly, were derived for surface-frozen monolayers of alkanes [15], closely resembling the present bilayer/liquid and bilayer/vapor interfaces for  $\phi = 0$ . The fit also yields a large 35% decrease in  $\gamma_{ls-OH}$ , and only a small 5% increase in  $\gamma_{ls-CH_3}$  over the range  $0 < \phi < 0.25$ ,

both as expected. However, the fit shows  $\gamma_{vl}(\phi)$ , the only directly measurable surface tension, to vary by  $\sim 13\%$  for  $0 < \phi < 0.2$ , in contrast with the measured 2%–3%. We conclude, therefore, that while a full quantitative agreement may require a more sophisticated theory, even the simple linear approximation employed here, which neglects mixing entropies and alcohol/diol repulsion [5], still captures the essentials of the physics underlying the phase diagram, with a minimal number of fit parameters.

We demonstrated here that the surface-frozen layers' structure in alcohols is tunable at the molecular level, by a judiciously chosen bulk additive. The unique bilayer/monolayer transition is driven by the  $\phi$  dependent balance of the surface free energies of the various phases, while the tilt changes result from the  $\phi$  variation of the subphase/layer interactions. Finally, we note that the surface freezing effect was thought [3,12,16] to be related to the existence of bulk rotator phases and, indeed, the surface layer's structure and phase diagram were found to follow those of the corresponding bulk rotator phases [3,12,16]. The monolayer phase found here is unique in having no correspondence to any of the bulk phases of alcohols. Implications of this for the possibility of molecular-level surface structure engineering await further exploration.

Beamtime at NSLS is gratefully acknowledged. BNL is supported by DOE Contract No. DE-AC02-98CH10886.

\*Email address: deutsch@alon.cc.biu.ac.il

- [1] X. Z. Wu *et al.*, Phys. Rev. Lett. **70**, 958 (1993).
- [2] X. Z. Wu *et al.*, Science **261**, 1018 (1993).
- [3] B. M. Ocko *et al.*, Phys. Rev. E **55**, 3164 (1997).
- [4] M. Deutsch *et al.*, Europhys. Lett. **30**, 283 (1995).
- [5] X. Z. Wu *et al.*, Phys. Rev. Lett. **75**, 1332 (1995).
- [6] O. Gang *et al.*, Phys. Rev. E **58**, 6068 (1998).
- [7] O. Gang *et al.*, Phys. Rev. Lett. **80**, 1264 (1998).
- [8] T. P. Russell, Mater. Sci. Rep. **5**, 171 (1990).
- [9] M. Deutsch and B. M. Ocko, in *Encyclopedia of Applied Physics*, edited by G. L. Trigg (Wiley, New York, 1998), Vol. 23, and references therein.
- [10] P. G. deGennes, Rev. Mod. Phys. **57**, 827 (1985).
- [11] O. Gang *et al.* (unpublished).
- [12] E. B. Sirota and X. Z. Wu, J. Chem. Phys. **105**, 7763 (1996).
- [13] V. M. Kaganer, H. Möhwald, and P. Dutta, Rev. Mod. Phys. (to be published).
- [14] Z. Wang, J. Phys. (Paris) **51**, 1431 (1990); A. Halperin, S. Alexander, and I. Schechter, J. Chem. Phys. **91**, 1383 (1981).
- [15] E. B. Sirota *et al.*, Phys. Rev. Lett. **79**, 531 (1997).
- [16] X. Z. Wu *et al.*, in *Dynamics in Small Confining Systems*, edited by J. M. Drake *et al.* (Materials Research Society, Pittsburgh, 1995), p. 15.